N.M.R. Study of Antiferromagnetic α-Mn Metal

Hideki Yamagata

OSAKA UNIVERSITY
GRADUATE SCHOOL OF ENGINEERING SCIENCE
TOYONAKA OSAKA

論 文 目 録

大阪大学

報告番号	第1971号	氏名	山 形 英 樹

主論文 N.M.R. Study ~~in~~ of Antiferromagnetic α-Mn Metal
(核磁気共鳴による反強磁性アルファマンガン金属の研究)
to be published in Journal of the Physical Society of Japan (1972).

参考論文 N.M.R. Study of Two Energy Gaps in Superconducting Compounds.
K.Asayama and H.Yamagata
J.Phys.Soc.Japan 22 (1967) 347.

N.M.R. in Al-Mn Alloys
Y.Oda, H,Yamagata and K.Asayama
J.Phys.Soc.Japan 25 (1968) 629.

Nuclear Magnetic Resonance in Antiferromagnetic α-Mn metals.
H.Yamagata and K.Asayama
J.Phys.Soc.Japan 29 (1970) 1385.

N.M.R. Study of Antiferromagnetic α-Mn Metal

Hideki Yamagata

December 1971

CONTENTS

Abstract

N.M.R. study has been made on antiferromagnetic α-Mn metal at helium temperature in zero external field. N.M.R. signals of Mn^{55} from Site I appear at 199.4 MHz. The signal from Site II consists of two split lines and appears at 151.5 and 144.5 MHz. The signals from Site III have complicated structure and appear in the range from 20 to 30 MHz. The signal from Site IV appears at around 5 MHz. It is concluded that there are two types of the magnetic moment on Site II. Their values are 1.85 and 1.75 μ_B respectively. Except for this point, the results are consistent with the recent neutron diffraction study and support the non-collinear spin configuration. The appearance of two types of moment at Site II is discussed.

§1. Introduction

The magnetic properties of 3d transition metals and alloys have been current interest for many physicists. Ferromagnetic iron group metals and alloys of such elements have been studied extensively by means of N.M.R. measurement to understand the electronic structure and the origin of ferromagnetism in these materials[1]. It is interesting to extend the measurements of N.M.R. to antiferromagnetic metals such as chromium and manganese.

The manganese metal has four metallic phases, that is, from low temperature, α-, β-, γ- and δ-phase. In α-, and γ-phase antiferromagnetism appears 95 K and 485 K respectively.

Alpha-manganese metal has a body-centered cubic lattice containing twenty-nine atoms per unit cell (fifty-eight atoms per cubic cell), in which the atoms occupy four inequivalent sites as follows: one atom in Site I, four atoms in Site II, twelve atoms in Site III and twelve atoms in Site IV as is shown in Fig.1[2].

Shull and Wilkinson first established the existence of antiferromagnetism of α-Mn with Neel temperature T_N=95 K by means of neutron diffraction method[3]. An analysis of the magnetic structure was also made by Kasper and Roberts with the powder sample below T_N[4]. They showed that the atoms in inequivalent sites have different moment and proposed two

types of possible magnetic structure. They are as follows:

A) 1.54 μ_B for Site I, 1.54 μ_B for II, 3.08 μ_B for III, and 0 μ_B for IV;

B) 2.50 μ_B for Site I, 2.50 μ_B for II, 1.70 μ_B for III, and 0 μ_B for IV.

An analysis of N.M.R. data above T_N by Jaccarino and Seitchik[5] favored model B. On the other hand Arrott and Cole, Sato and Arrott explained the mechanismof antiferromagnetism in α-Mn by static spin density wave[6].

The hyperfine field measurement of α-Mn is very interesting. However there have been few experiments about it[7][8], since the methods of measurement developed for ferromagnetic metals are not easily applicable to antiferromagnetic metals. Zero field N.M.R. is the best tool for measuring the hyperfine field. It is determined from the following relation

$$h\omega_o = \mu_n H_n / I \qquad (1\text{-}1)$$

where ω_o is the resonance angular frequency, μ_n is the nuclear magnetic moment, I is the nuclear spin number, and H_n is the hyperfine field. Zero field N.M.R. signal in antiferromagnetic α-Mn metal has already been observed at around 5 MHz[7]. From this the hyperfine field on α-Mn was determined to be 4.8 KOe. On the other hand, the hyperfine field determined from nuclear specific heat measurement is 90 KOe[8] and supported the model B by Kasper and Roberts. Recently Yamada succeeded in growing a large single crystal of α-Mn[9] and Yamada, Kunitomi, Nakai, Fujii, Cox and Shirane made a neutron diffraction experiment on it[10] and Yamada analyzed

the magnetic structure with systematic method [11]. According to them, the magnetic moments on Site I, II, III and IV are 1.9, 1.7, 0.6 and 0.25 μ_B respectively and the magnetic structure is described by a non-collinear configuration. The magnetic structure determined by Yamada et al. is shown in Fig.2. Therefore the N.M.R. signal around 5 MHz can be attributed to the nuclei that belong to Site IV.

We constructed a high power spin echo apparatus with variable frequency and succeeded to detect new N.M.R. signals that correspond to Site I, II and III. This paper presents new N.M.R. signals in details.

§2. Experimental procedure

The sample supplied by Yamada and Kunitomi is the same one as that used in neutron scattering study[10]. Its purity is 99.99 %. The ingot was crushed into powder in argon atmosphere to prevent the oxidization. The powder was coated with paraphine to prevent oxidization and to keep the insulation between particles to avoid the lowering of the Q value of the sample coil by eddy current loss. The high value of Q is very effective in sensitivity in high frequency region (higher than 30 MHz).

The experiment was carried out by spin echo method, which is convenient to detect an inhomogeneously broadened resonance spectrum. In zero field N.M.R. of ferromagnet an enhancement mechanism resulting from induced oscillations of domain walls plays an important role for detection of the resonance. This enhancement is not likely to be present in antiferromagnet in zero external field. Thus it is necessary to construct high power pulsed oscillator and highly sensitive receiver system in order to observe the N.M.R. signal of antiferromagnetic metal in zero external field. In V.H.F. region especially above 60 MHz, it becomes considerably difficult to obtain high power. But one can obtain high power oscillating field H_1 by using the apparatus shown in Fig.3. Using this apparatus N.M.R. signals of Mn nuclei in antiferromagnetic Cr-Mn alloys have also been observed[12]. The measurement was performed at 1.4 and 4.2 K far below the Neel temperature, and in the frequency range between 15 MHz and 230 MHz. The temperatures were

determined from liquid helium vapor pressure. H_1 used is about 20 Oe. The line shape was obtained from echo amplitude varying the oscillator frequency. Echo amplitude depends on the separation between 90^o and 180^o pulses as follows:

$$A(\tau)=A_o\exp(-2\tau/T_2) \qquad (2\text{-}1)$$

where τ is the separation between two pulses, T_2 is transverse relaxation time and $A(\tau)$ is the measured echo amplitude. Since T_2 is different at each frequency, echo amplitudes extraporated to $\tau=0$, A_o, are used to obtain the line shape. Repetition time of echo measurements was chosen to be much longer than the spin lattice relaxation time T_1. The value of H_1 was kept as constant as possible over the frequency range in the present experiment.

§3. Experimental results

N.M.R. signals are observed at around 30 MHz, 145 MHz and 200 MHz in addition to the signal at around 5 MHz that has been already observed[7]. The intensity ratio of the signals at 5 MHz and 30 MHz is determined to be nearly one by comparing the integrated area of these signals. Here the difference in sensitivity at different resonance frequencies is corrected by the proton resonance in water. It is consistent with the fact that the number of atoms at Site III is equal to that at Site IV. According to the neutron scattering study, the magnetic moment of Site III is larger than that of Site IV. It is natural, therefore, to assign the N.M.R. signal at around 5 MHz to that from the nuclei at Site IV and the N.M.R. signal at around 30 MHz to that from nuclei at Site III. The N.M.R. intensity at around 145 MHz and 200 MHz could not be corrected by proton resonance because of the lack of suitable external field. However from rough intensity measurement and the consideration of the magnitude of the magnetic moment, it is determined reasonably that the N.M.R. signal at 200 MHz is that from the nuclei at Site I and the N.M.R. signals distributed at around 145 MHz is that from the nuclei at Site II.

a) Mn^{55} resonance at Site I (written as Mn^{55}-I).
The resonance line from Mn^{55}-I is single and narrow as is shown in Fig.4. It is consistent with the fact that there is no electric field gradient at Mn^{55}-I and this site is magnetically symmetric point as shown in Fig.1 and Fig.2.

The centre of resonance frequency is 199.4 MHz. From the relation (1-1) and using μ_n/hI=10.5 MHz/10^4Oe[13], the hyperfine field is determined to be 190 KOe. Transverse relaxation time T_2 is very short compared with that of Site III and IV and temperature independent in the region from 1.4 to 4.2 K.

b) Mn^{55}-II resonance.

Resonance lines from Mn^{55}-II are widely distributed and have two peaks as are shown in Fig.5. From these two peaks, the hyperfine fields are determined to be 137.6 and 144.3 KOe respectively. Intensity ratio of these two lines is about one. There is an axially symmetric field gradient at Mn^{55}-II. The atoms at Site II have the same magnetic moment according to the neutron scattering study[10]. These two peaks cannot be explained by the single value of the magnetic moment. It is reasonable to conclude that there are two different hyperfine fields corresponding to two types of the magnetic moments. Detailed discussion will be given in §4.

c) Mn^{55}-III resonance.

Resonance lines from Mn^{55}-III are widely distributed and have complicated structure as are shown in Fig.6. From large two peaks the hyperfine fields are determined as 25.7 KOe and 29.5 KOe. According to the results of the neutron diffraction study[10] which are reproduced in Table I there are two types of magnetic moment on this site, and also an asymmetric electric field gradient is produced at this site[14]. Detailed discussion about the hyperfine fields and magnetic moments on this site will be given in §4.

d) Mn^{55}-IV resonance.

In Fig.7, the frequency distribution of the resonance line of Mn^{55}-IV is reproduced from reference (7). The line shape has asymmetry and although split lines are not observed, it seems that there exist two peaks at around 7.1 KOe and 4.8 KOe respectively. Also an asymmetric field gradient is expected at this site[14]. But the signal intensity at this site is much weaker than that of Site III and any complicated structure cannot be well resolved.

The results of N.M.R. are shown in Table I, together with the values of the magnetic moment determined by neutron diffraction study[10]. In the analysis of the neutron data, the absolute value of the magnetic moment depends on the choice of the magnetic form factor. A number of form factors were assumed by Yamada et al. which were constructed from the Freeman-Watson values for 3d and 4s electrons in the manganese atoms. They are as follows:

$$\left.\begin{aligned} f_1 &= 1/0.8(f_{3d} - 0.2f_{4s}) \\ f_2 &= 1/0.9(f_{3d} - 0.1f_{4s}) \\ f_3 &= f_{3d} \\ f_4 &= 1/1.1(f_{3d} + 0.1f_{4s}) \\ f_5 &= 1/1.2(f_{3d} + 0.2f_{4s}) \end{aligned}\right\} \qquad (3\text{-}1)$$

The magnetic moments calculated by use of the form factor f_1, f_2 or f_3 fitted the experiment. The values given in Table I are the magnetic moment associated with the form factor f_2. The internal fields are plotted against the corresponding magnetic moments in Fig.8.

Site	N	$\mu(f_2)$ (in μ_B)	H_n (in KOe)
I	1	2.05	190
II	4	1.79	144.3
			137.6
III	4	0.62	29.5
	8	0.57	25.7
IV	4	0.22	7.1
	8	0.31	4.8

Table I. The number of atoms N, the magnetic moment $\mu(f_2)$ associated with the form factor f_2 in unit of Bohr magneton and internal field H_n in each site of α-Mn.

§4. Discussion and conclusion

Hyperfine field is different for each of four inequivalent sites. This result is consistent with the neutron diffraction study by Yamada et al.[10] and inconsistent with that of Kasper and Roberts[4]. As is shown in Fig.8, the internal field is not in linear relation with the magnitude of the magnetic moment. This non-linear property may be attributed to the following origins.

(1) In the analysis by Yamada et al. , the form factor is assumed to be common for all sites. There may be a possibility that the form factor is different for each site and the real magnitudes of the magnetic moments are somewhat different from that given by their analysis.

(2) The ratio of the s-d mixing may be different for different sites corresponding to the difference in the form factor, resulting in non-linearity of the internal field with the magnetic moment.

(3) The contribution to the hyperfine field from the moment on other sites may be taken into account and the magnetic moment is not necessarily proportional to the hyperfine field

The neutron diffraction results are explained assuming that the magnetic moment on Site II is of one Kind. But present experiment shows that there are two types of hyperfine field in this site. The line width of the lower line is larger than that of the higher line. Even if the contributions from the neighbouring moments are taken into account to the internal field as scalar and dipolar type the resonance line at Site II

is single and does not split into two lines. As for the interpretation on N.M.R. spectra on Site II shown in Fig.5, we consider as follows:

a) These two kinds of hyperfine field correspond to two types of moment and the atom with the larger moment has a larger hyperfine field. The numbers of atoms of these two kinds are two and two.

b) In the case of existence of the electric field gradient, N.M.R. spectra of nuclei of the spin number I=5/2 split into five lines as shown in Fig.9 (a). Each of two resonances arising from Site II consists of these five lines and the separation of the adjacent lines Δ_q may be different for these two resonances. If we assume an inhomogeneous line width, δ, for each of five lines, these five lines will overlap to produce a single broad line, and two broad peaks with different widths are expected for the resonance of Site II nuclei.

The separation Δ_q is expressed as

$$\Delta_q = \frac{e^2qQ}{h} \frac{3}{2I(2I-1)} \frac{1}{2}(3\cos^2\theta - 1) \qquad (4\text{-}1)$$

where q is the electric field gradient, Q is the nuclear quadrupole moment, θ is the angle between the direction of hyperfine field and the principal axis of the electric field gradient. As the quadrupole coupling constant e^2qQ/h is the same for each four atoms on Site II, the difference in Δ_q is attributed to the difference of θ. Varying the line width δ of each of five lines and the separation Δ_q, we obtain the values of δ and Δ_q which give best fit to the observed spectra.

Here the line shape of the each five line is assumed to be Gaussian. These values are

$$\left.\begin{aligned}\delta_1 &= 1.2 \text{ (MHz)}\\ \Delta_{q_1} &= 0.5 \text{ (MHz)}\end{aligned}\right\} \text{ for the higher frequency line}$$

$$\left.\begin{aligned}\delta_2 &= 1.2 \text{ (MHz)}\\ \Delta_{q_2} &= 0.8 \text{ (MHz)}\end{aligned}\right\} \text{ for the lower frequency line.}$$

Comparison of the calculated line shape with N.M.R spectrum is shown in Fig.9 (b).

Corresponding to the hyperfine fields 144.3 and 137.6 KOe, we separate the magnitude of the magnetic moments on Site II into two kinds. This separation may not be unique because there exist several reasons for the non-linear relation between the hyperfine field and the magnetic moment as discussed previously. We assume that the internal field is proportional to the magnetization on Site II, and using the values of 1.79 μ_B and 141 KOe for the average value of hyperfine field we separate the moments into two types as $\mu_{II-1}=1.84$ and $\mu_{II-2}=1.75$ μ_B respectively. The results obtained on Site II is shown in Table II.

Site	N	μ_{II}(in μ_B)	H_n (KOe)	δ (MHz)	Δ_q(MHz)
II-1	2	1.84	144.3	1.2	0.5
II-2	2	1.75	137.6	1.2	0.8

Table II. Data on Site II of magnetic moment μ_{II}, hyperfine field H_n, line width δ and line seperation Δ_q and the number of atoms N.

According to the above discussion, we conclude that

(1) There are two types of magnetic moment on Site II.

(2) θ is different for each of two kinds of the moment and the nuclei with larger moment have smaller Δ_q.

These results are not explained by the neutron diffraction results which show the magnetic moment to be of one kind 1.79 μ_B and θ has the same value $27^\circ 28'$ for all four atoms as is shown in Fig.10. In the neutron diffraction study, the magnetic structure of α-Mn was analyzed by only the vector basis function $f^{(2)}$ belonging to irreducible representation $_F(2)$ 10).

We reproduce here briefly the analysis of Yamada. This is as follows:

The magnetic structure is described by thermal average of magnetization $\vec{M}(\vec{r})$ at the point $\vec{r}$ in the crystal. Only the magnetization $\vec{M}(\vec{r})$ that minimize the internal energy E

$$E = -\frac{1}{2}\iint \vec{M}(\vec{r})J(\vec{r},\vec{r}')\vec{M}(\vec{r}')d^3\vec{r}\ d^3\vec{r}' \qquad (4\text{-}2)$$

should be present in the crystal. The tensor $J(\vec{r},\vec{r}')$ is invariant against operation of the space group in the crystal. When the magnetization $\vec{M}(\vec{r})$ and $\vec{M}(\vec{r}')$ in formula (4-2) are expanded in the space of vector basis functions for the irreducible representations of the space group, the energy given by formula (4-2) is diagonal with respect to these representations, i.e. $\vec{M}(\vec{r})$ and $\vec{M}(\vec{r}')$ couple only when they belong to the same representation.

The vector basis functions are constructed by the following procedure. Scalar quantities of the crystal are most conveniently expressed by the scalar basis functions of the irreducible representations of the space group. We consider first a scalar quantity which is a function of the positions of the atoms on the crystal; an asymmetrized function can be taken as

$$\phi(\vec{r};\vec{q},\vec{r}_{jn}) = \sum_m \exp(i\vec{q}\cdot\vec{R}_m)\,\delta(\vec{r}-\vec{r}_{jn}-\vec{R}_m) \qquad (4\text{-}3)$$

for each $\vec{r}_{jn}$, where q is a reciprocal vector within the first Brillouin zone, $\vec{r}_{jn}$ is the position of j-th atom of Site n in the unit cell, $\vec{R}_m$ is the position of the center of m-th cell, so that the atom position in the crystal is $\vec{r}=\vec{R}_m-\vec{r}_{jn}$.

These functions have to be symmetrized with respect to the point group of wave vector $\vec{q}=(1,0,0)$[11),17)]. This point group is a subgroup. Only the atom number j in the function changes under operations of the point group. We have sets of symmetrized functions, for $\vec{q}=(1,0,0)$ and for each site, of the form

$$\phi^{(\vec{q},\alpha,n)}=\sum_m \exp(i\vec{q}\cdot\vec{R}_m)\sum_j c_j^{(\vec{q},\alpha,n)}\delta(\vec{r}-\vec{r}_{jn}-\vec{R}_m) \qquad (4-4)$$

where $\phi^{(q,\alpha,n)}$ is a linear combination of the functions given by eq. (4-3). The $c_j^{(q,\alpha,n)}$ are a basis for the α-th irreducible representation of the group of q for Site n. The number of times $b^{(\alpha)}$ the α-th representations contained in the reducible representation based on the functions given by eq. (4-3) is given by

$$b^{(\alpha)} = (1/g)\sum_G \chi(G)\chi^{\alpha}(G)^* \qquad (4-5)$$

where G represents an element of the point group of dimension g, $\chi(G)$ is the character of the reducible representation, and $\chi^{\alpha}(G)^*$ is the character of α-th irreducible representation (an asterisk indicates conjugate complex). Consulting the symmetry type of each representation given in the character

table, we can write down the coefficient $c_j^{(q,\alpha,n)}$.

We present here for the point group T_d only the groups of the wave vectors at $\vec{q}=(1,0,0)$ and at $\vec{q}=(0,0,0)$ (i.e. the H and Γ points in the zone). The characters of T_d are shown in Table III, and the numbers $b^{(\alpha)}$ based on the scalar basis are given in the middle column of Table IV. The coefficients $c_j^{(\vec{q},\alpha,n)}$ for these values of q are given in Table V.

	E	$8C_3$	$3C_2$	6_d	$6S_4$
$A^{(1)}$	1	1	1	1	1
$A^{(2)}$	1	1	1	-1	-1
E	2	-1	2	0	0
$F^{(2)}$	3	0	-1	1	-1
$F^{(1)}$	3	0	-1	-1	1

Table III. The character table for T_d.

We take the symbol for representations from Landau and Lifshitz[15]. We use the corresponding small letter to specify the basis function of the representation. If there are two representations, for example the two $F^{(2)}$ for Site III (also for Site IV), they are distinguished by writing $F^{(2)-1}$ and $F^{(2)-2}$.

Table IV. The number on scalar and vector basis.

Site	Scalar basis		Vector basis (Polar)	
I	$A^{(1)}$	1	$F^{(2)}$	1
II	$A^{(1)}$	1	$A^{(1)}$	1
	$F^{(2)}$	1	E	1
			$F^{(2)}$	2
			$F^{(1)}$	1
III and IV	$A^{(1)}$	1	$A^{(1)}$	2
	E	1	$A^{(2)}$	1
	$F^{(2)}$	2	E	3
	$F^{(1)}$	1	$F^{(2)}$	5
			$F^{(1)}$	4

Table V. The value of $c_j^{(\alpha,n)}$. $\beta=\sqrt{1/2}$, $\gamma=\sqrt{3/2}$.

Site n	$\phi^{(\alpha)}$	Atom-number j											
		1	2	3	4	5	6	7	8	9	10	11	12
I	$a^{(1)}$	1											
II	$a^{(1)}$	1	1	1	1								
	$f_1^{(2)}$	-1	1	1	-1								
	$f_2^{(2)}$	1	-1	1	-1								
	$f_3^{(2)}$	1	1	-1	-1								
III and IV	$a^{(1)}$	1	1	1	1	1	1	1	1	1	1	1	1
	e_1	-2β	β	β	-2β	β	β	-2β	β	β	-2β	β	β
	e_2	0	γ	$-\gamma$	0	γ	$-\gamma$	0	γ	$-\gamma$	0	γ	$-\gamma$
	$f_1^{(2)-1}$	1	1	1	-1	-1	-1	-1	-1	-1	1	1	1
	$f_2^{(2)-1}$	1	1	1	-1	-1	-1	1	1	1	-1	-1	-1
	$f_3^{(2)-1}$	1	1	1	1	1	1	-1	-1	-1	-1	-1	-1
	$f_1^{(2)-2}$	β	β	-2β	$-\beta$	$-\beta$	2β	$-\beta$	$-\beta$	2β	β	β	-2β
	$f_2^{(2)-2}$	β	-2β	β	$-\beta$	2β	$-\beta$	β	-2β	β	$-\beta$	2β	$-\beta$
	$f_3^{(2)-2}$	-2β	β	β	-2β	β	β	2β	$-\beta$	$-\beta$	2β	$-\beta$	$-\beta$
	$f_1^{(1)}$	γ	$-\gamma$	0	$-\gamma$	γ	0	$-\gamma$	γ	0	γ	$-\gamma$	0
	$f_2^{(1)}$	$-\gamma$	0	γ	γ	0	$-\gamma$	$-\gamma$	0	γ	γ	0	$-\gamma$
	$f_3^{(1)}$	0	γ	$-\gamma$	0	γ	$\pm\gamma$	0	$-\gamma$	γ	0	$-\gamma$	γ

We take an orthogonal set of unit vectors, $\vec{i}, \vec{j}$, and $\vec{k}$, along the axis of the cubic lattice. A vector quantity in the crystal is expressed as $\vec{v}(\vec{r})=v_1(\vec{r})\vec{i}+v_2(\vec{r})\vec{j}+v_3(\vec{r})\vec{k}$. If we use the scalar basis functions as the components of $\vec{v}(\vec{r})$, the resultant set of $\vec{v}(\vec{r})$'s constitutes a basis for a reducible representation of the space group. That is a direct product of the representations in the space of the scalar basis functions and in the space of $\vec{i}$, $\vec{j}$, $\vec{k}$.

In the case of the point group T_d, the set $\vec{i}$, $\vec{j}$, and $\vec{k}$ constitutes the basis of $F^{(2)}$. Irreducible representations based on the vector basis are found by decomposing the direct product

$$\begin{aligned} A^{(1)} \times F^{(2)} &= F^{(2)} \\ A^{(2)} \times F^{(2)} &= F^{(1)} \\ E \times F^{(2)} &= F^{(1)} + F^{(2)} \\ F^{(2)} \times F^{(2)} &= A^{(1)} + E + F^{(1)} + F^{(2)} \\ F^{(1)} \times F^{(2)} &= A^{(2)} + E + F^{(1)} + F^{(2)} \end{aligned} \qquad (4\text{-}6)$$

The number $b^{(\alpha)}$ for the irreducible representations based on the vector basis is given in the right column of Table IV. The vector basis functions are constructed in the following form:

$$\vec{a}^{(1)} = (1/3)^{1/2}(f_1^{(2)}\vec{i}+f_2^{(2)}\vec{j}+f_3^{(2)}\vec{k}) \qquad (4\text{-}7)$$

$$\vec{a}^{(2)} = (1/3)^{1/2}(f_1^{(1)}\vec{i}+f_2^{(1)}\vec{j}+f_3^{(1)}\vec{k}) \qquad (4\text{-}8)$$

$$\left.\begin{aligned} \vec{e}^{1}_{1} &= (1/6)^{1/2}(-f_1^{(2)}\vec{i}-f_2^{(2)}\vec{j}+2f_3^{(2)}\vec{k}) \\ \vec{e}^{1}_{2} &= (1/2)^{1/2}(f_1^{(2)}\vec{i}-f_2^{(2)}\vec{j}) \end{aligned}\right\} \qquad (4\text{-}9)$$

$$\left.\begin{aligned}\vec{e}^{2}{}_{1}&=(1/2)^{1/2}(f_1^{(1)}\vec{i}-f_2^{(1)}\vec{j})\\ \vec{e}^{2}{}_{2}&=(1/6)^{1/2}(-f_1^{(1)}\vec{i}-f_2^{(1)}\vec{j}+2f_3^{(1)}\vec{k})\end{aligned}\right\}\quad(4\text{-}10)$$

$$\left.\begin{aligned}\vec{f}_1^{(2)-1}&=a^{(1)}\vec{i}\\ \vec{f}_2^{(2)-1}&=a^{(1)}\vec{j}\\ \vec{f}_3^{(2)-1}&=a^{(1)}\vec{k}\end{aligned}\right\}\quad(4\text{-}11)$$

$$\left.\begin{aligned}\vec{f}_1^{(2)-2}&=(-\tfrac{1}{2}e_1+\tfrac{3}{2}e_2)\vec{i}\\ \vec{f}_2^{(2)-2}&=(-\tfrac{1}{2}e_1-\tfrac{3}{2}e_2)\vec{j}\\ \vec{f}_3^{(2)-2}&=e_1\vec{k}\end{aligned}\right\}\quad(4\text{-}12)$$

$$\left.\begin{aligned}\vec{f}_1^{(2)-3}&=(1/2)^{1/2}(f_3^{(2)}\vec{j}+f_2^{(2)}\vec{k})\\ \vec{f}_2^{(2)-3}&=(1/2)^{1/2}(f_1^{(2)}\vec{k}+f_3^{(2)}\vec{i})\\ \vec{f}_3^{(2)-3}&=(1/2)^{1/2}(f_2^{(2)}\vec{i}+f_1^{(2)}\vec{j})\end{aligned}\right\}\quad(4\text{-}13)$$

$$\left.\begin{aligned}\vec{f}_1^{(2)-4}&=(1/2)^{1/2}(f_3^{(1)}\vec{j}-f_2^{(1)}\vec{k})\\ \vec{f}_2^{(2)-4}&=(1/2)^{1/2}(f_1^{(1)}\vec{k}-f_3^{(1)}\vec{i})\\ \vec{f}_3^{(2)-4}&=(1/2)^{1/2}(f_2^{(1)}\vec{i}-f_1^{(1)}\vec{j})\end{aligned}\right\}\quad(4\text{-}14)$$

$$\left.\begin{aligned}\vec{f}_1^{(1)-1}&=a^{(2)}\vec{i}\\ \vec{f}_2^{(1)-1}&=a^{(2)}\vec{j}\\ \vec{f}_3^{(1)-1}&=a^{(2)}\vec{k}\end{aligned}\right\}\quad(4\text{-}15)$$

$$\left.\begin{aligned}\vec{f}_1^{(1)-2}&=(-\tfrac{3}{2}e_1-\tfrac{1}{2}e_2)\vec{i}\\ \vec{f}_2^{(1)-2}&=(\tfrac{3}{2}e_1-\tfrac{1}{2}e_2)\vec{j}\\ \vec{f}_3^{(1)-2}&=e_2\vec{k}\end{aligned}\right\}\quad(4\text{-}16)$$

$$\vec{f}_1^{(1)-3}=(1/2)^{1/2}(f_3^{(2)}\vec{j}-f_2^{(2)}\vec{k})$$
$$\vec{f}_2^{(1)-3}=(1/2)^{1/2}(f_1^{(2)}\vec{k}-f_3^{(2)}\vec{i}) \qquad (4\text{-}17)$$
$$\vec{f}_3^{(1)-3}=(1/2)^{1/2}(f_2^{(2)}\vec{i}-f_1^{(2)}\vec{j})$$

$$\vec{f}_1^{(1)-4}=(1/2)^{1/2}(f_3^{(1)}\vec{j}+f_2^{(1)}\vec{k})$$
$$\vec{f}_2^{(1)-4}=(1/2)^{1/2}(f_1^{(1)}\vec{k}+f_3^{(1)}\vec{i}) \qquad (4\text{-}18)$$
$$\vec{f}_3^{(1)-4}=(1/2)^{1/2}(f_2^{(1)}\vec{i}+f_1^{(1)}\vec{j})$$

Some representative modes, for example "arrow" distributions in Site II, that are given by eq. (4-7) to (4-18) are illustrated in Fig.12.

We observe in Table IV that only the representation $F^{(2)}$ (on the vector basis) is common to all sites; $A^{(2)}$, E, $F^{(2)}$ and $F^{(1)}$ are common to Site II, III and IV; and $A^{(2)}$ is contained only in Site III and IV.

Here it is assumed that the magnetic structure is simple and is expressed by the vector basis function belonging to only one irreducible representation. The irreducible representation which we have to take is $F^{(2)}$ if Site I has non-zero magnetic moment . If the moment on Site I is zero, the representation is not uniquely determined. It is reasonable to assume that Site I has a non-zero magnetic moment. As a result $F^{(2)}$ must be considered.

The vector basis functions of representation $F^{(2)}$ are given by the formula (4-11) to (4-14). Combining these functions for each site, we get

$$
\left.
\begin{aligned}
\vec{m}_1(\vec{r}) = &\left[\sum_{n=I}^{IV} v_n a^{(1)}(\vec{r};n) + \sum_{n=III}^{IV} z_n\left\{-\frac{1}{2}e_1(\vec{r};n) + \frac{\sqrt{3}}{2}e_2(\vec{r};n)\right\}\right]\vec{i} \\
&+\left[\sum_{n=II}^{IV} w_n f_3^{(2)-1}(\vec{r};n) + \sum_{n=III}^{IV}\left\{x_n f_3^{(2)-2}(\vec{r};n) + y_n f_3^{(1)}(\vec{r};n)\right\}\right]\vec{j} \\
&+\left[\sum_{n=II}^{IV} w_n f_2^{(2)-1}(\vec{r};n) + \sum_{n=III}^{IV}\left\{x_n f_2^{(2)-2}(\vec{r};n) - y_n f_2^{(1)}(\vec{r};n)\right\}\right]\vec{k} \\
\vec{m}_2(\vec{r}) = &\left[\sum_{n=II}^{IV} w_n f_3^{(2)-1}(\vec{r};n) + \sum_{n=III}^{IV}\left\{x_n f_3^{(2)-2}(\vec{r};n) - y_n f_2^{(1)}(\vec{r};n)\right\}\right]\vec{i} \\
&+\left[\sum_{n=I}^{IV} v_n a^{(1)}(\vec{r};n) + \sum_{n=III}^{IV} z_n\left\{-\frac{1}{2}e_1(\vec{r};n) - \frac{3}{2}e_2(\vec{r};n)\right\}\right]\vec{j} \\
&+\left[\sum_{n=II}^{IV} w_n f_1^{(2)-1}(\vec{r};n) + \sum_{n=III}^{IV}\left\{x_n f_1^{(2)-2}(\vec{r};n) + y_n f_1^{(1)}(\vec{r};n)\right\}\right]\vec{k} \\
\vec{m}_3(\vec{r}) = &\left[\sum_{n=II}^{IV} w_n f_2^{(2)-1}(\vec{r};n) + \sum_{n=III}^{IV}\left\{x_n f_2^{(2)-2}(\vec{r};n) + y_n f_2^{(1)}(\vec{r};n)\right\}\right]\vec{i} \\
&+\left[\sum_{n=II}^{IV} w_n f_1^{(2)-1}(\vec{r};n) + \sum_{n=III}^{IV}\left\{x_n f_1^{(2)-2}(\vec{r};n) - y_n f_1^{(1)}(\vec{r};n)\right\}\right]\vec{j} \\
&+\left[\sum_{n=I}^{IV} v_n a^{(1)}(\vec{r};n) + \sum_{n=III}^{IV} z_n e_1(\vec{r};n)\right]\vec{k}
\end{aligned}
\right\} \qquad (4\text{-}19)
$$

where v_n, w_n, x_n, y_n and z_n are parameters, and $a^{(1)}(r;n)$ etc. are the scalar basis functions for Site n. We have the following parameters:

$$
\left.
\begin{aligned}
&v_I && \text{for Site I;} \\
&v_{II} \text{ and } w_{II} && \text{for Site II;} \\
&v_{II},\ w_{II},\ x_{II},\ y_{II} \text{ and } z_{II} && \text{for Site II;} \\
&v_{IV},\ w_{IV},\ x_{IV},\ y_{IV} \text{ and } z_{IV} && \text{for Site IV;}
\end{aligned}
\right\} \qquad (4\text{-}20)
$$

To choose between the structures represented by $\vec{m}_1$, $\vec{m}_2$, $\vec{m}_3$, is identical to choose the pricipal axis of the magnetization. A torque measurement on α-Mn has shown that it is the $\langle 100 \rangle$ direction[16]. As a result, the magnetic structure is

$$\vec{M}(\vec{r}) = \vec{m}_3(\vec{r}) \qquad (4\text{-}21)$$

Using the values of thirteen parameters determined from neutron scattering study and eq. (4-21), the magnetic structure was determined as is shown in Fig.2.
The above discussion is survey about Yamada's discussion.

In the case of Yamada's analysis, it is assumed that the magnetic structure of α-Mn is simple and can be described by the vector basis function belonging to only one irreducible representation $F^{(2)}$. But present results on Site II cannot be explained by it and can be explained by adding to $F^{(2)}$ a small amount of vector basis function belonging to irreducible representation E. The magnetic moment on Site II can be split into two parts by adding either vector basis function $\vec{a}^{(1)}$ or $\vec{e}$ to $\vec{f}^{(2)}$. But the case of adding $\vec{a}^{(1)}$ into $\vec{f}^{(2)}$ is contrary to the present results that the atom with a larger moment has a larger θ (the angle between the direction of moment and electric field gradient).Then we consider only the case of adding $\vec{e}$ to $\vec{f}^{(2)}$. Then the magnetization $\vec{M}'(\vec{r})$ is written by using the eq. (4-9) and (4-10) as

$$\vec{M}'(\vec{r}) = \vec{m}_3(\vec{r}) + \sum_{n=II}^{IV} s_n \vec{e}^1{}_1 + \sum_{n=III}^{IV} t_n \vec{e}^1{}_1 + \sum_{n=III}^{IV} u_n \vec{e}^2{}_1 \qquad (4\text{-}22)$$

where s_n, t_n and u_n are new parameters for the vector basis functions belonging to representation E. Each component of magnetization $\vec{M}'(\vec{r})$ is shown in Table VI. The differences in magnitude of the magnetic moment and angle Θ between the pairs on Site II depend on s_n, a ratio of the mixing amount of the vector basis function $\vec{e}$ to $\vec{f}^{(2)}$.

The magnitude of two magnetic moments on Site II are

$$\left.\begin{aligned} \mu_{II_1} &= \sqrt{2(w_{II}+\alpha s_{II})^2+(v_{II}+2\alpha s_{II})^2}\times 1.33\mu_B \quad \text{for } j=1,2 \\ \mu_{II_2} &= \sqrt{2(w_{II}-\alpha s_{II})^2+(v_{II}-2\alpha s_{II})^2}\times 1.33\mu_B \quad \text{for } j=3,4 \\ \alpha &= \sqrt{1/6}. \qquad\qquad\qquad\qquad (\text{at } 4.4\text{K}) \end{aligned}\right\} \quad (4\text{-}23)$$

Site n	j	$\vec{i}$	$\vec{j}$	$\vec{k}$
I	1	0	0	v_n
II	1	$w_n+\alpha s_n$	$-w_n-\alpha s_n$	$v_n+2\alpha s_n$
	2	$-w_n-\alpha s_n$	$w_n+\alpha s_n$	$v_n+2\alpha s_n$
	3	$w_n-\alpha s_n$	$w_n-\alpha s_n$	$v_n-2\alpha s_n$
	4	$-w_n+\alpha s_n$	$-w_n+\alpha s_n$	$v_n-2\alpha s_n$

Table VI-(a). The $\vec{i}$-, $\vec{j}$- and $\vec{k}$-components of magnetic moment for Site I and II, where $\alpha=\sqrt{1/6}$.

n	j	$\vec{i}$	$\vec{j}$	$\vec{k}$
III and IV	1	$w_n+\beta x_n-\gamma y_n$ $-\alpha s_n-\alpha\beta t_n+\beta\gamma u_n$	$w_n+\beta x_n- y_n$ $-\alpha s_n-\alpha\beta t_n+\beta\gamma u_n$	$v_n-2\beta z_n$ $-2\alpha s_n-4\alpha\beta t_n$
	2	$w_n-2\beta x_n$ $-\alpha s_n-\alpha\beta t_n-\beta\gamma u_n$	$w_n-\beta x_n-\gamma y_n$ $-\alpha s_n+2\alpha\beta t_n$	$v_n+\beta z_n$ $+2\alpha s_n+2\alpha\beta t_n$
	3	$w_n+\beta x_n+\gamma y_n$ $-\alpha s_n+2\alpha\beta t_n$	$w_n-2\beta x_n$ $-\alpha s_n-\alpha\beta t_n-\beta\gamma u_n$	$v_n+\beta z_n$ $+2\alpha s_n+2\alpha\beta t_n$
	4	$-w_n-\beta x_n+\gamma y_n$ $+\alpha s_n+\alpha\beta t_n-\beta\gamma u_n$	$-w_n-\beta x_n+\gamma y_n$ $+\alpha s_n+\alpha\beta t_n-\beta\gamma u_n$	$v_n-2\beta z_n$ $+2\alpha s_n-4\alpha\beta t_n$
	5	$-w_n+2\beta x_n$ $+\alpha s_n+\alpha\beta t_n+\beta\gamma u_n$	$-w_n-\beta x_n-\gamma y_n$ $+\alpha s_n-2\alpha\beta t_n$	$v_n+\beta z_n$ $+2\alpha s_n+2\alpha\beta t_n$
	6	$-w_n-\beta x_n-\gamma y_n$ $+\alpha s_n-2\alpha\beta t_n$	$-w_n+2\beta x_n$ $+\alpha s_n+\alpha\beta t_n+\beta\gamma u_n$	$v_n+\beta z_n$ $+2\alpha s_n+2\alpha\beta t_n$
	7	$w_n+\beta x_n- y_n$ $+\alpha s_n+\alpha\beta t_n-\beta\gamma u_n$	$-w_n-\beta x_n+\gamma y_n$ $-\alpha s_n-\alpha\beta t_n+\beta\gamma u_n$	$v_n-2\beta z_n$ $-2\alpha s_n+4\alpha\beta t_n$
	8	$w_n-2\beta x_n$ $+\alpha s_n+\alpha\beta t_n+\beta\gamma u_n$	$-w_n-\beta x_n-\gamma y_n$ $-\alpha s_n+2\alpha\beta t_n$	$v_n+\beta z_n$ $-2\alpha s_n-2\alpha\beta t_n$
	9	$w_n+\beta x_n+\gamma y_n$ $+\alpha s_n-2\alpha\beta t_n$	$-w_n+2\beta x_n$ $-\alpha s_n-\alpha\beta t_n-\beta\gamma u_n$	$v_n-\beta z_n$ $-2\alpha s_n-2\alpha\beta t_n$
	10	$-w_n-\beta x_n+\gamma y_n$ $-\alpha s_n-\alpha\beta t_n+\beta\gamma u_n$	$w_n+\beta x_n-\gamma y_n$ $+\alpha s_n+\alpha\beta t_n-\beta\gamma u_n$	$v_n-2\beta z_n$ $-2\alpha s_n+4\alpha\beta t_n$
	11	$-w_n+2\beta x_n$ $-\alpha s_n-\alpha\beta t_n-\beta\gamma u_n$	$w_n+\beta x_n+\gamma y_n$ $+\alpha s_n-2\alpha\beta t_n$	$v_n+\beta z_n$ $-2\alpha s_n-2\alpha\beta t_n$
	12	$-w_n-\beta x_n-\gamma y_n$ $-\alpha s_n+2\alpha\beta t_n$	$w_n-2\beta x_n$ $+\alpha s_n+\alpha\beta t_n+\beta\gamma u_n$	$v_n+\beta z_n$ $-2\alpha s_n-2\alpha\beta t_n$

Table VI. The $\vec{i}$-, $\vec{j}$- and $\vec{k}$-components of magnetic moment for Site III and IV, where $\alpha=\sqrt{1/6}$, $\beta=\sqrt{1/2}$, $\gamma=\sqrt{3/2}$.

As the difference in the magnitudes of two moments is very small, i.e the mixing is small, this difference could not be detected in the neutron scattering experiment[17]. This situation is shown schematically in Fig.13. Quantitative comparison of the calculated ratio of the quadrupole splittings, $\Delta_{q_1}/\Delta_{q_2}$, from the above analysis to produce two different moments, with that determined from N.M.R. line spectrum is done as follows. By varying value of the parameter s_{II}, we obtained for the value of s_{II} of $0.08\times1.33\ \mu_B$ the calculated values of μ_{II_2}, μ_{II_1} which fit best our experimental data. The values are 1.85 and 1.75 μ_B for μ_{II_2} and μ_{II_1} respectively. Here we assume that s_{II} is positive and use the values of $v_{II}=-1.199\times1.33\mu_B$ and $w_{II}=0.437\times1.33\mu_B$ for the form factor f_2 in (3-1)[10]. By the admixture of E, the angle θ_1 and θ_2 corresponding to magnetic moments 1.75 and 1.85 μ_B become different and for the above value of s_{II} these two θ's are calculated to be $24^\circ21'$ and $30^\circ25'$ respectively. From these values and eq. (4-1), the ratio $\Delta_{q_1}/\Delta_{q_2}$ becomes 1.2. On the other hand, the values in the last column of Table II obtained from N.M.R. spectrum, gives this ratio to be 1.6. But because of uncertainties in various assumptions the agreement seems qualitatively good.

The above argument that a small part of E should mix to $F^{(2)}$ to interpret the existence of two moments on Site II fives four types of the magnetic moment on both Site III and IV[11),17]. The atoms having these four different moments are two atoms with atom number j=1,4, two atoms with j=7,10, four atoms with j=2,3,5,6 and four atoms with

j=8,9,11,12 respectively both for Site III and IV as is shown in Table VI and Fig.13. The analysis become complicated in this case due to the existence of the asymmetric electric field gradient and the increase of the kind of moment by adding e to $f^{(2)}$. One possible explanation of the complicated spectra in Fig.6 may be as follows. By the introduction of the $\vec{e}$ mode, the magnetic moment is devided into four groups as mentioned above.Consulting with the structure symmetry, the equivalent atoms with regard to the direction of the electric field gradient, q and asymmetric factor, η, are further classified into pairs of 1,4, 7,10, 2,5, 3,6, 8,11 and 9,12, where atoms 8,9,11,12 and 2,3,5,6 have the same magnetic moment, respectively. We assume that the signals from two pairs, for example 2,5 and 3,6 appear at 31 MHz, two pairs 8,11 and 9,12 appear around 27 MHz, one pair for example 1,4 happens to have large electric quadrupole splitting due to a proper angle, the central line appearing at 23 MHz, and finally the last pair 7,10 has similar splitting and partially overlaps with the lines from 1,4 and from 8,11 and 9,12 as is shown in Fig.14 (3). If the magnitude of the splitting is chosen as 1.6 MHz, the complicated structure in Fig.6 is consistently explained as is shown in Fig.15. This value is reasonable with the magnitude of the pure quadrupole frequency of 1.638 MHz for Site III (or Site IV) and 1.488 MHz for Site IV (or SiteIII) determined by Andersson in paramagnetic α-Mn[14].

These results may suggest that the magnetic structure of α-Mn is not simple, being unable to be expressed by one base function. This may suggests that there exist more

than two mechanisms for occurence of the spontaneous magnetization on α-Mn. One is explained by the interaction between localized d-electrons. Another probable mechanism is the same as one for appearence of weak ferromagnetism in MnB_2[18]. It is as follows: There are two types of electron state, i.e. localized d-electron and itinerant s-electron. The magnetic structure of the unperturbed system is primarily determined by the direct interaction between each localized d-electrons. Now if a polarization of conduction electron occurs, a tilting of the localized spin is induced through the s-d exchange interaction. This may be the present case.

Finally, we comment on the hyperfine field. The value of the root mean square of the hyperfine field on each site amount to 65.6 KOe. This value is somewhat smaller than the values of 90 KOe determined by the nuclear specific heat measurement[8]. The ratio of the hyperfine field and magnetic moment amounts to 75 KOe/μ_B, where magnetic moment used is 0.87 μ_B obtained by taking a root mean square for each site. This value is nearly the same as the value of manganese in antiferromagnetic Cr-Mn alloys, 80 KOe/u_B[12].

The values of the quadrupole coupling constant e^2qQ/h on Site II is estimated to be about 6 MHz using the eq. (4-1). Here the average values of θ and Δ_q are used as $27^\circ 28'$ and 0.65 MHz respectively.

Acknowledgement

The author wishes to express his thanks to professors J.Itoh and K.Asayama for their cotinuous guidance and encouragements. He is also indebted to professors T.Yamada and N.Kunitomi for helpful discussions and suggestions and supplying α-Mn sample. The present study was also facilitated by help of Mr.H.Takenaka.

Reference

1) A.M.Portis and R.H.Lindquist: "Magnetism II A" edited by G.T.Rado and H.Suhl, Academic Press p.357 (1965).

2) A.J.Bradley and J.Thewlis: Proc. Roy. Soc. A115 (1927) 456.

3) C.G.Shull and M.K.Wilkinson: Rev. Mod. Phys. 25 (1953) 100.

4) J.S.Kasper and B.W.Roberts: Phys. Rev. 101 (1956) 537.

5) V.Jaccarino and J.A.Seitchik: Bull. Amer. Phys. Soc. 10 (1965) 317.

6) A.Arrott and B.R.Coles: J. appl. Phys. 32 (1961) 51S.
H.Sato and A.Arrott: J. Phys. Soc. Japan 17B-I (1962) 147.

7) J.Itoh, Y.Masuda, K.Asayama and S.Kobayashi: J. Phys. Soc. Japan. 18 (1963) 455.

8) R.G.Scurlock and W.N.R.Stevens: Proc. Phys. Soc. 86 (1965) 331.

9) T.Yamada: J. Phys. Soc. Japan. 28 (1970) 1499.

10) N.Kunitomi, T.Yamada, Y,Nakai and Y.Fujii: j. appl. Phys. 40 (1969) 1265.
T.Yamada, N.Kunitomi, Y.Nakai, D.E.Cox and G.Shirane: J. Phys. Soc. Japan 28 (1970) 615.

11) T.Yamada: J. Phys. Soc. Japan 28 (1970) 596.

12) H.Takenaka and K.Asayama: J. phys. Soc. Japan 31 (1971) 299.

13) W.B.Mins, G.E.Devlin, S.Gesehwind and V.Jaccarino: Phys. Letters. 24A (1967) 481.

14) L.O.Andersson: Phys. Letters 26A (1968) 279.

15) L.D.Landau and E.M.Lifshits: "Quantum Mechanics" (Pergamon Press, Oxford, 1965) p.332.

16) T.Yamada and S.Tazawa: J. Phys. Soc. Japan 28 (1970) 609.

17) T.Yamada: private communication.
T.Yamada and N.Kunitomi: Bussei 5 (1971) 249.

18) M.Kasaya and T.Hihara: J. Phys. Soc. Japan 29 (1970) 336.

Figure Captions

Fig.1. Crystal lattice (upper in the figure) and the atomic configuration in a cell. The centre of cube in every site corresponds to Site I. The number on each atom indicates atom number j as same as in reference (10) and ((11). The length of each cube is indicated with an unit in a lattice constant of α-Mn.

Fig.2. Magnetic structure of α-Mn. The length of each cube corresponds to $\vec{i}$-, $\vec{j}$- and $\vec{k}$-component of magnetic moment in unit of μ_B for the form factor f_2.

Fig.3. Circuit of high power pulsed oscillator used at around 30 MHz. This circuit is also useful for higher frequency by changing the suitable coils and oscillator tubes.

Fig.4. The Mn^{55} resonance spectra in Site I observed by spin echo method at 1.4 K. The number indicated in a parenthesis is hyperfine field.

Fig.5. The Mn^{55} resonance spectra in Site II observed by spin echo method at 1.4 K. The number indicated in a parenthesis is hyperfine field.

Fig.6. The Mn^{55} resonance spectra in Site III observed at 4.2 K.

Fig.7. The Mn^{55} resonance spectra in Site IV reproduced from the reference (7).

Fig.8. Hyperfine field against the magnetic moment in unit of KOe and Bohr magneton (μ_B) respectively. Solid curve obtained from joining the ponits at the averaged value of hyperfine field and magnetic moment on each site. The point on Site II indicated with the triangle (Δ) is that modified by present work.

Fig.9. a). The resonance spectrum when electric field gradient is present in the case of nuclear spin number I=5/2. The number in lower part is an intensity ratio of the resonance spectrum.

b). Comparison the observed resonance spectra in Site II (solid curve) with composed line (dotted line). The dotted lines are normalized at poit indicated in an arrows.

Fig.10. Relation between magnetic moment and electric field gradient for Site II. The magnetic moments on j=1,2 and on j=3,4 are present on the planes d_1 and d_2 respectively.

Fig.11. Representative modes expressed by the vector basis fuctions for Site II.

Fig.12. Circumstances for changing the magnitude of the magnetic moment and the direction after and before adding a vector basis function $\vec{e}$ into $\vec{f}^{(2)}$ for Site II. The dotted line indicates the state after the change.

Fig.13. Circumstances for changing the magnitude of magnetic moment before and after adding a vector basis function $\vec{e}$ into $\vec{f}^{(2)}$ for Site III shown in (a) and (b) respectively. The group with same mark has the same magnitude in the magnetic moment.

Fig.14. Circumstances for changing the line spectra on Site III after and before adding $\vec{e}$ mode to $\vec{f}^{(2)}$ are shown.

(1). The line spectra before adding $\vec{e}$. The line indicated with open circle and triangle correspond to the signals from the atoms with j=1,4,7,10 and j=2,3,5,6,8, 9,11,12 respectively.

(2). The line spectra after adding e. Each two lines are devided into two lines from j=1,4 and 7,10 and from j=2,3,5,6 and 8,9,11,12 respectively.

(3). Two lines (lower frequency side) are devided into five lines respectively due to electric quadrupole effect and construct seven lines. The double open circles indicate a center of frequency in the five lines.

Fig.15. Comparison of the explanation in Fig.14 with experimental spectra (solid curve) on Site III. The length of the bars corresponds to the intensity normalized at lowest peak. The bars with same sign are correspond to same group atoms.

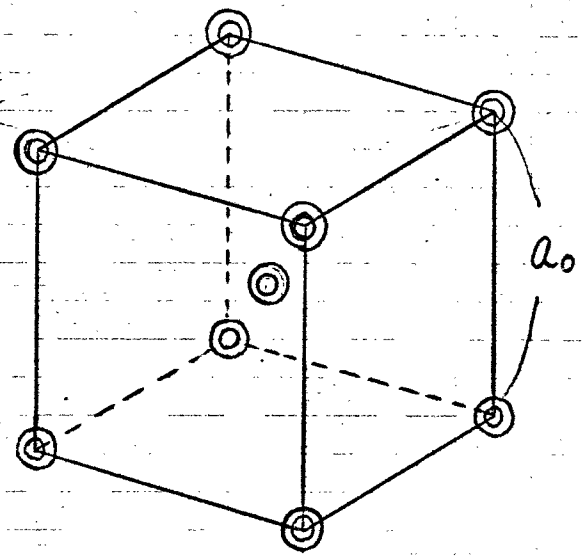

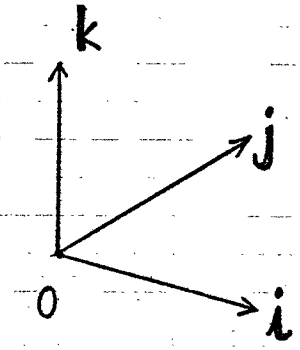

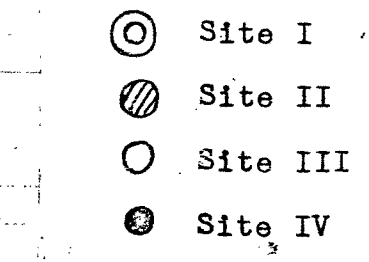

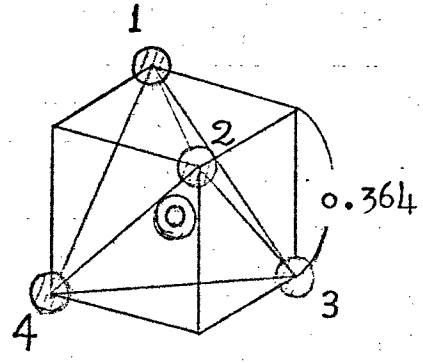

Site I, II

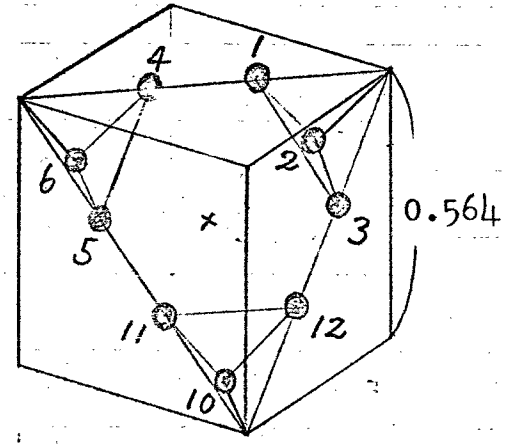

Site IV

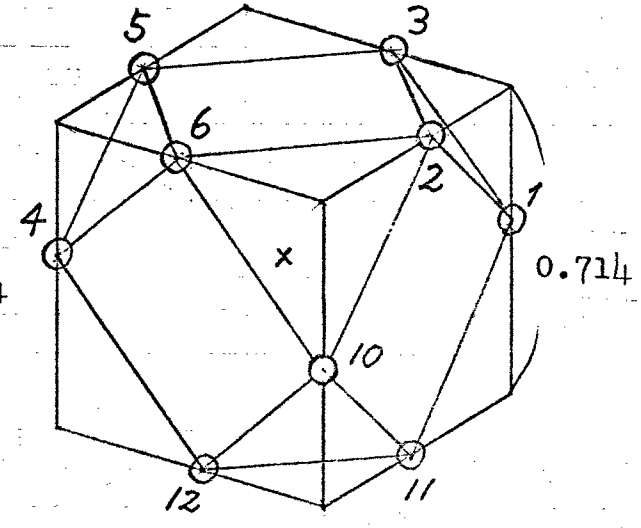

Site III

Fig 1

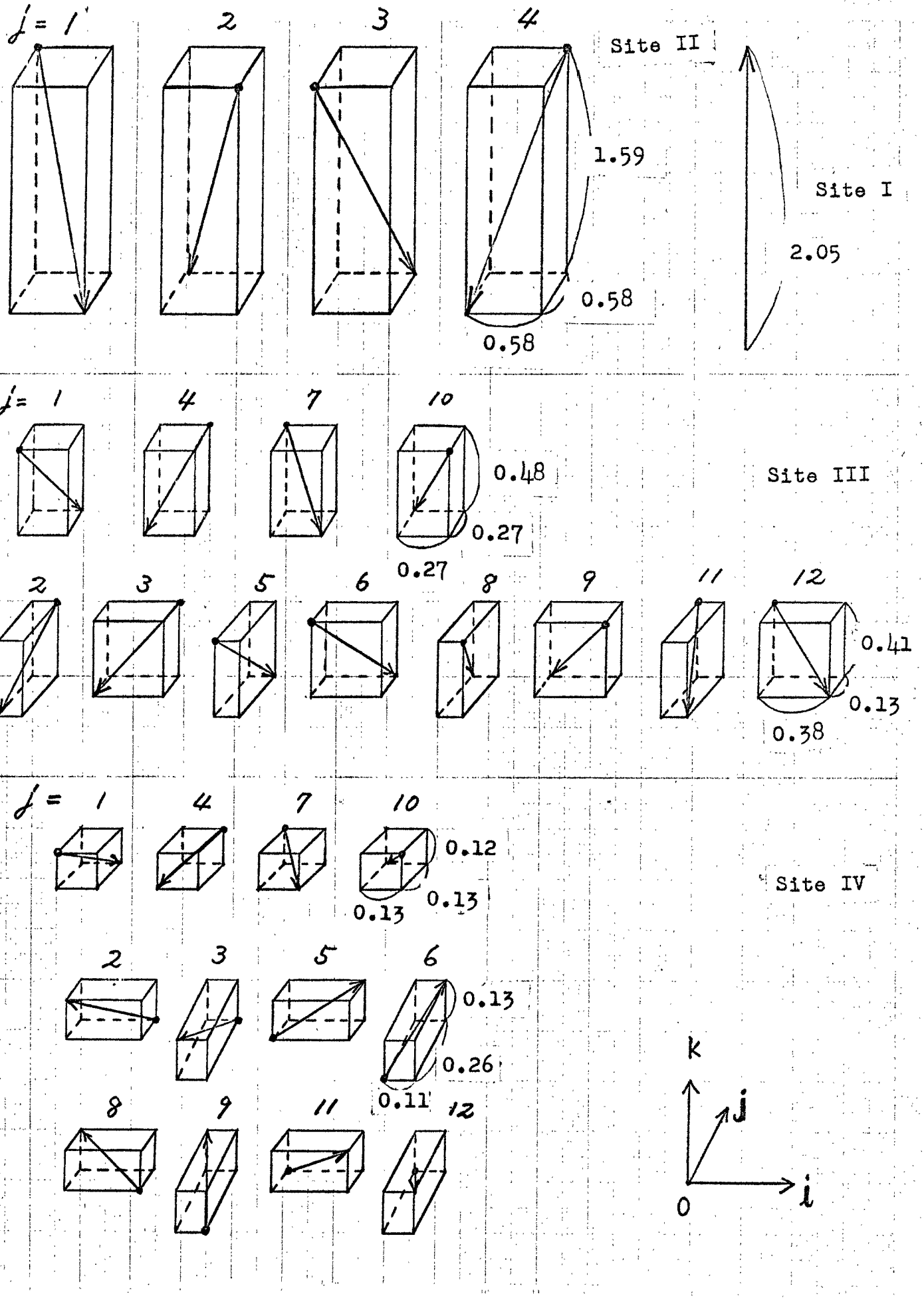
j = 1
2
3
4
Site II
1.59
0.58
0.58
Site I
2.05
j = 1
4
7
10
0.48
0.27
0.27
Site III
2
3
5
6
8
9
11
12
0.41
0.13
0.38
j = 1
4
7
10
0.12
0.13
0.13
Site IV
2
3
5
6
0.13
0.26
0.11
8
9
11
12
k
j
i
0

Fig 2

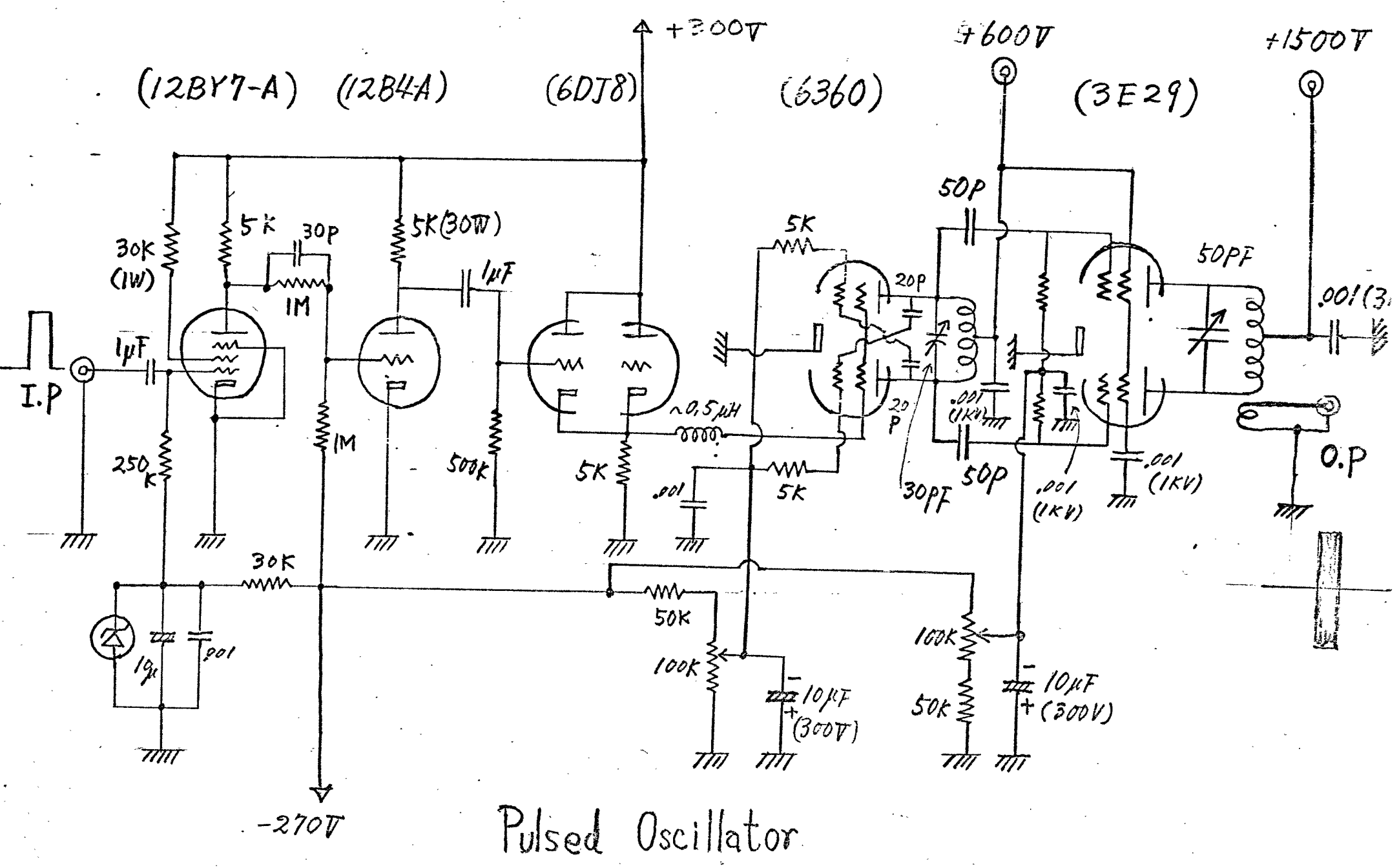

Pulsed Oscillator

Fig 3

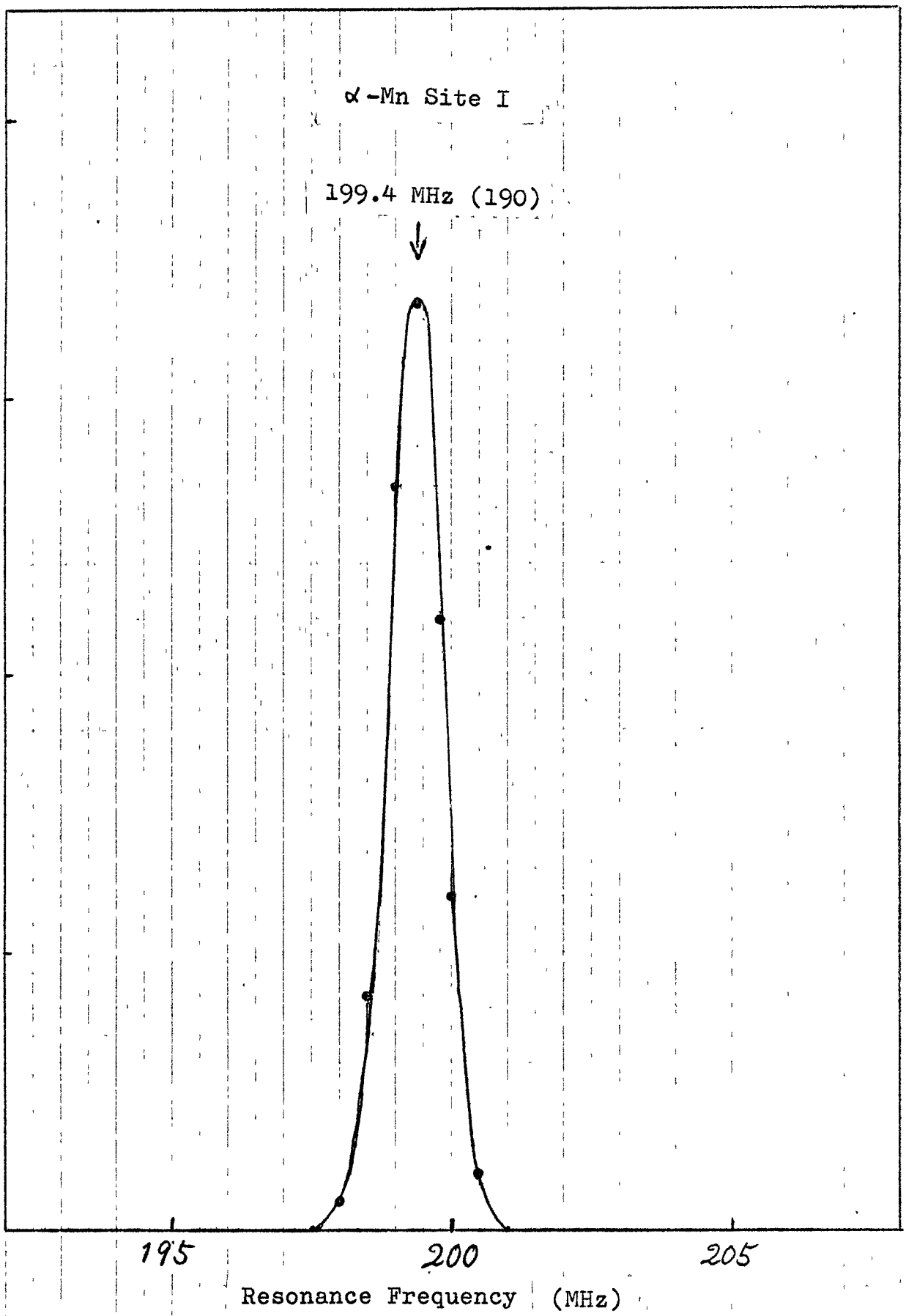
α-Mn Site I
199.4 MHz (190)
Echo Intensity
195
200
205
Resonance Frequency (MHz)

Fig 4

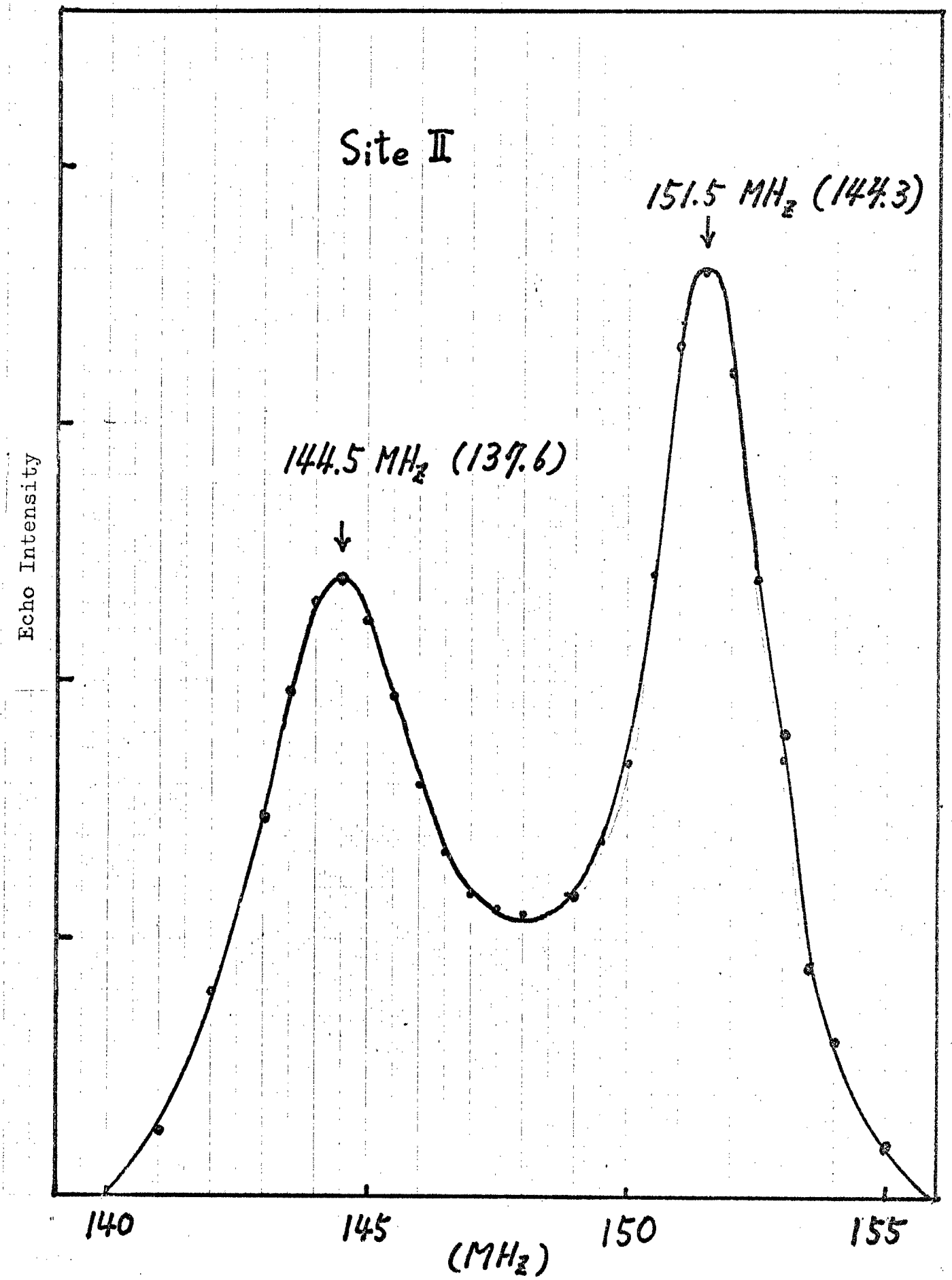
Site II
151.5 MHz (144.3)
144.5 MHz (137.6)
Echo Intensity
140
145
150
155
(MHz)

Fig. 5

Fig. 6

Echo Intensity
15
20
25
30
35
40
(MHz)
Site III
26.5 MHz (25.7)
31 MHz (29.5)

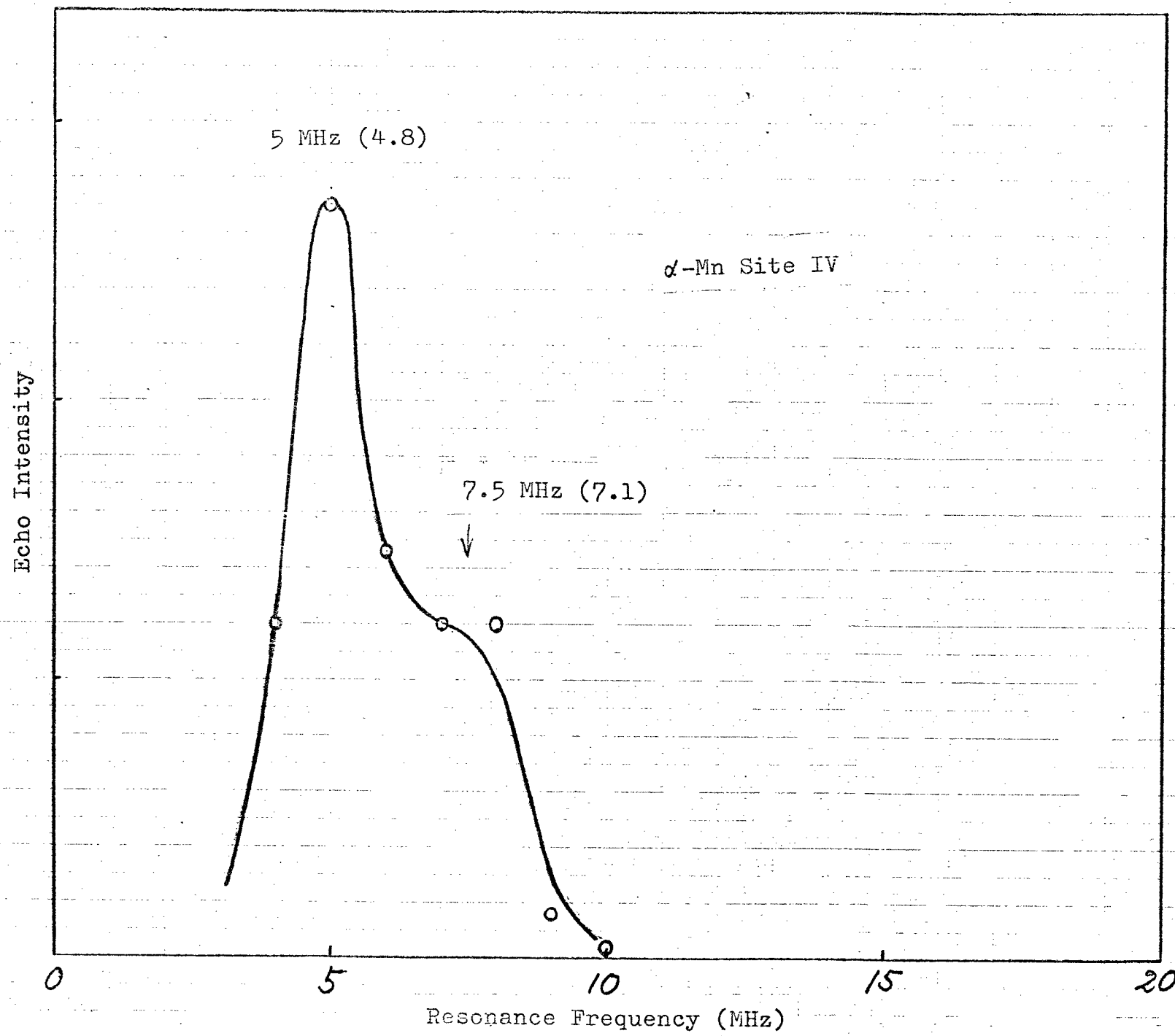
5 MHz (4.8)
α-Mn Site IV
7.5 MHz (7.1)
Echo Intensity
0
5
10
15
20
Resonance Frequency (MHz)

Fig 9

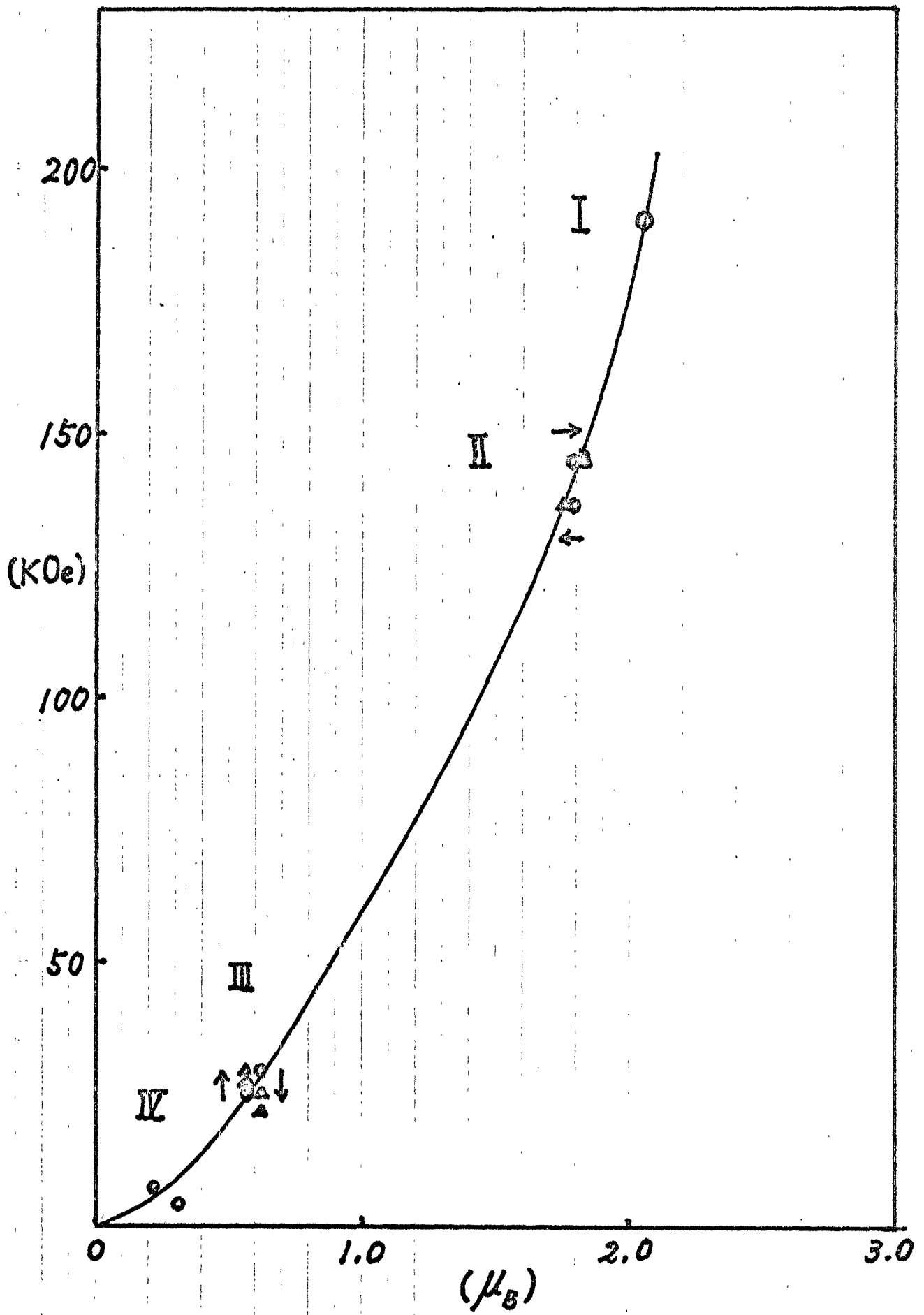

Fig. 8

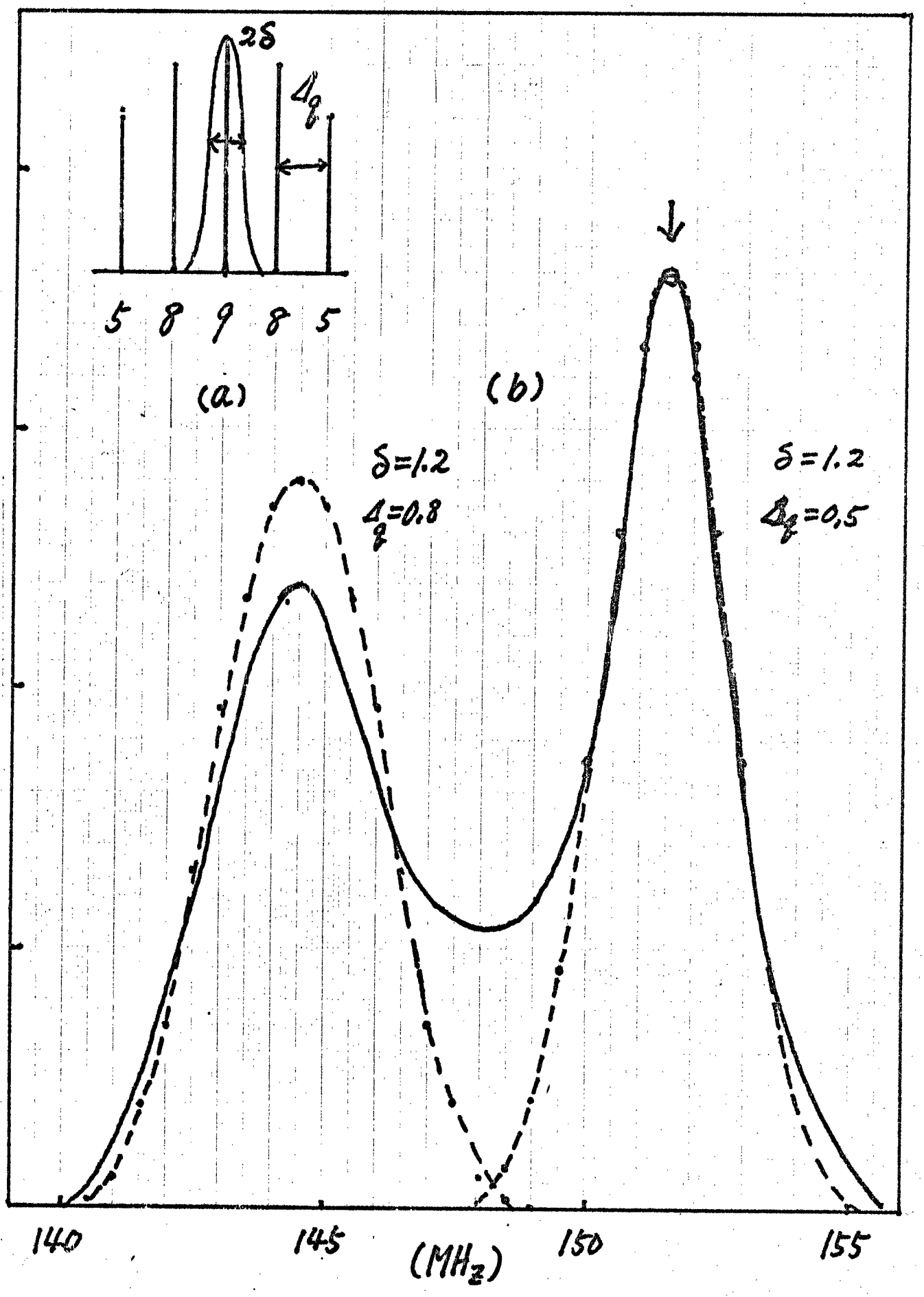
2δ
Δ_g
5 8 9 8 5
(a)
(b)
δ=1.2
Δ_g=0.8
δ=1.2
Δ_g=0,5
Echo Intensity
140
145
150
155
(MHz)

Fig. 9

Fig 10

(a)

(b)

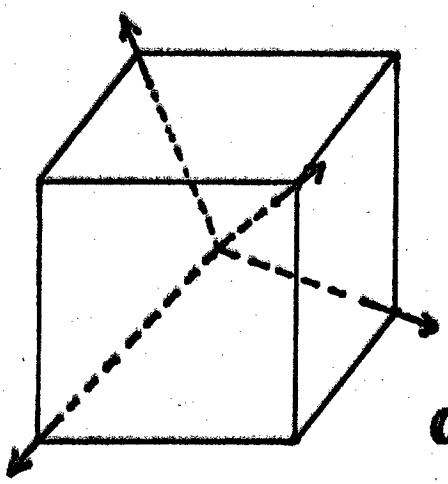

$a^{(1)}$

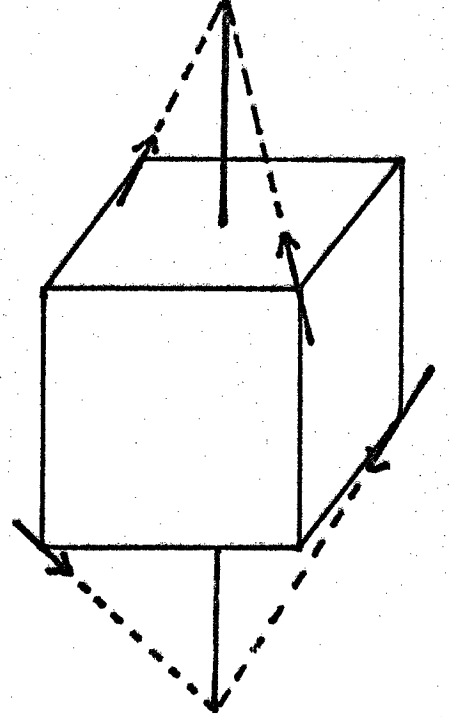

e_1

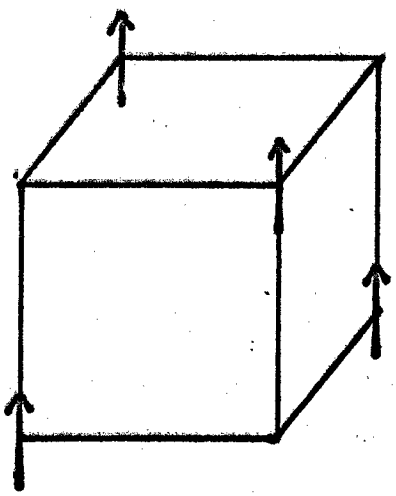

$f_3^{(2)-1}$

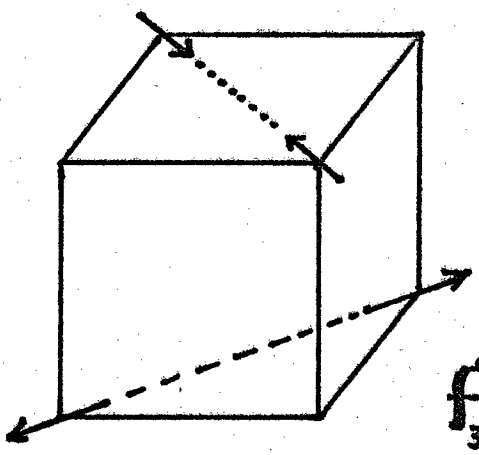

$f_3^{(2)-3}$

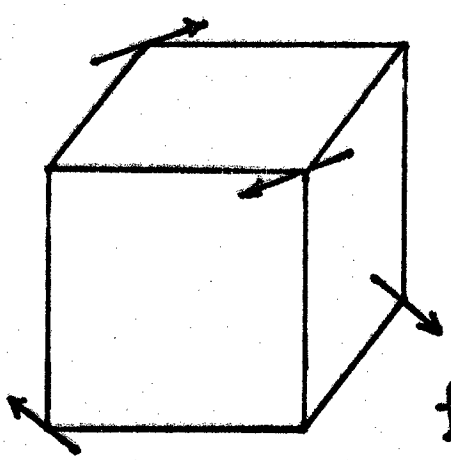

$f_3^{(1)}$

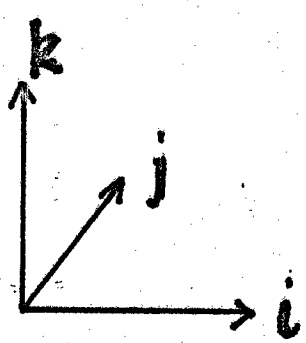

Fig 11

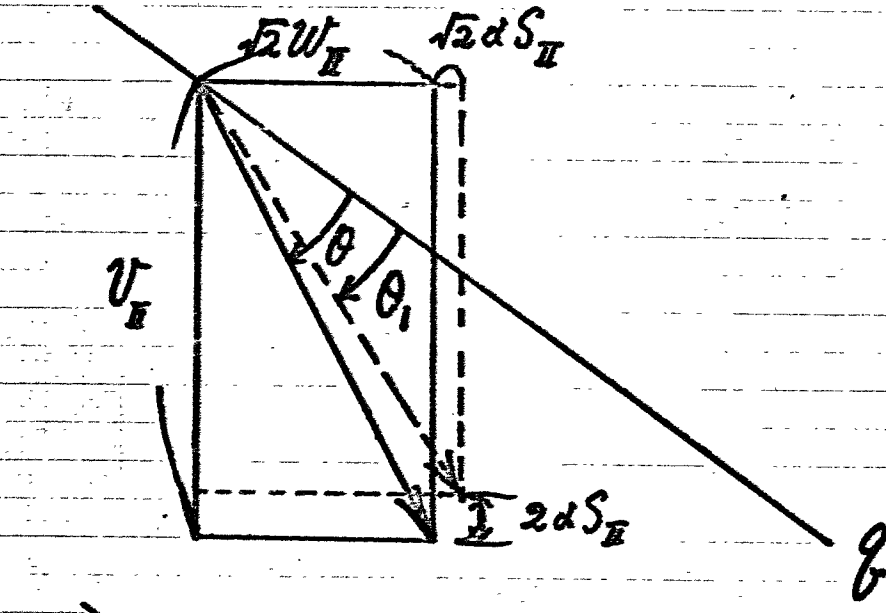

for $j = 1, 2.$

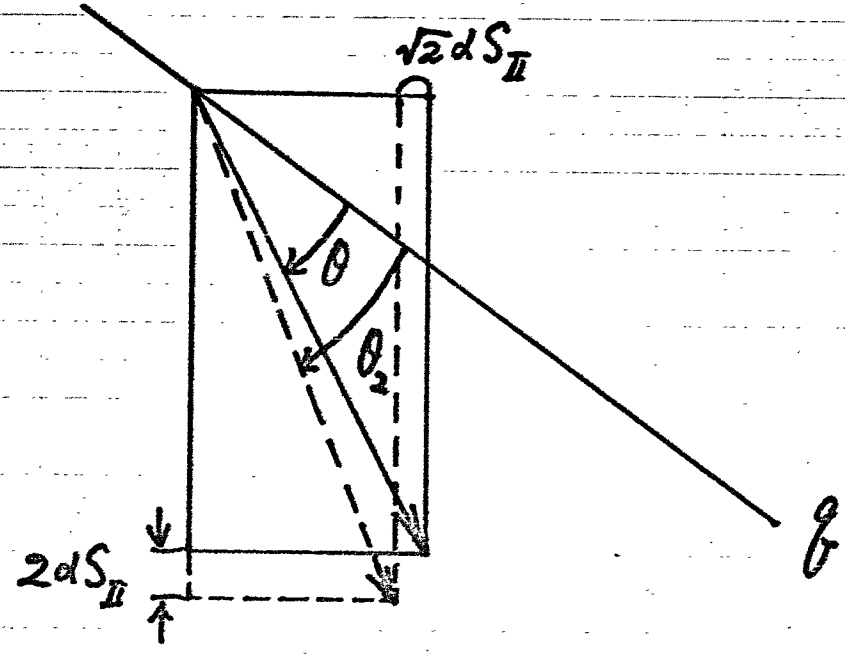

for $j = 3, 4.$

Fig. 12

Fig. 13.

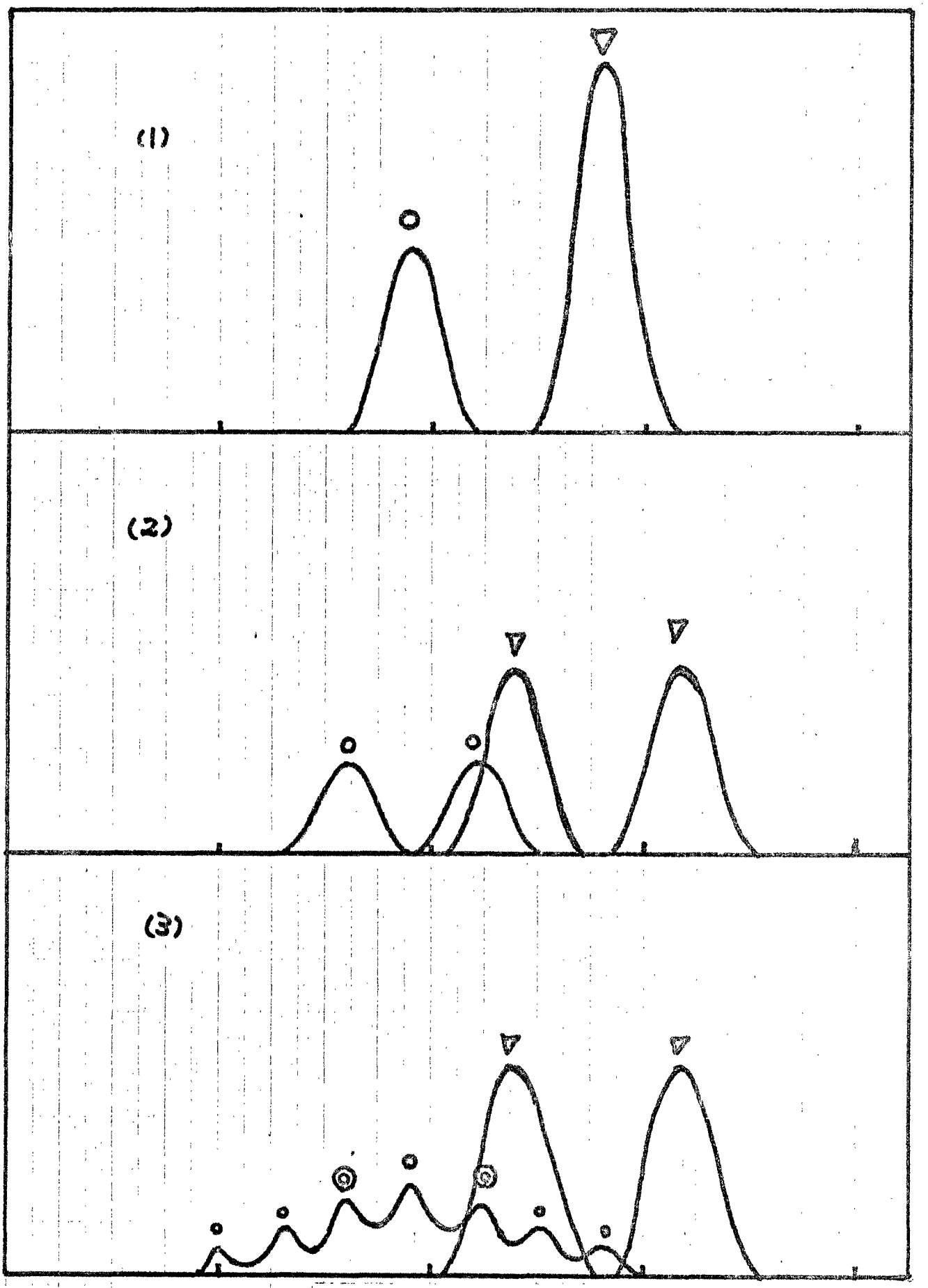

Fig 14

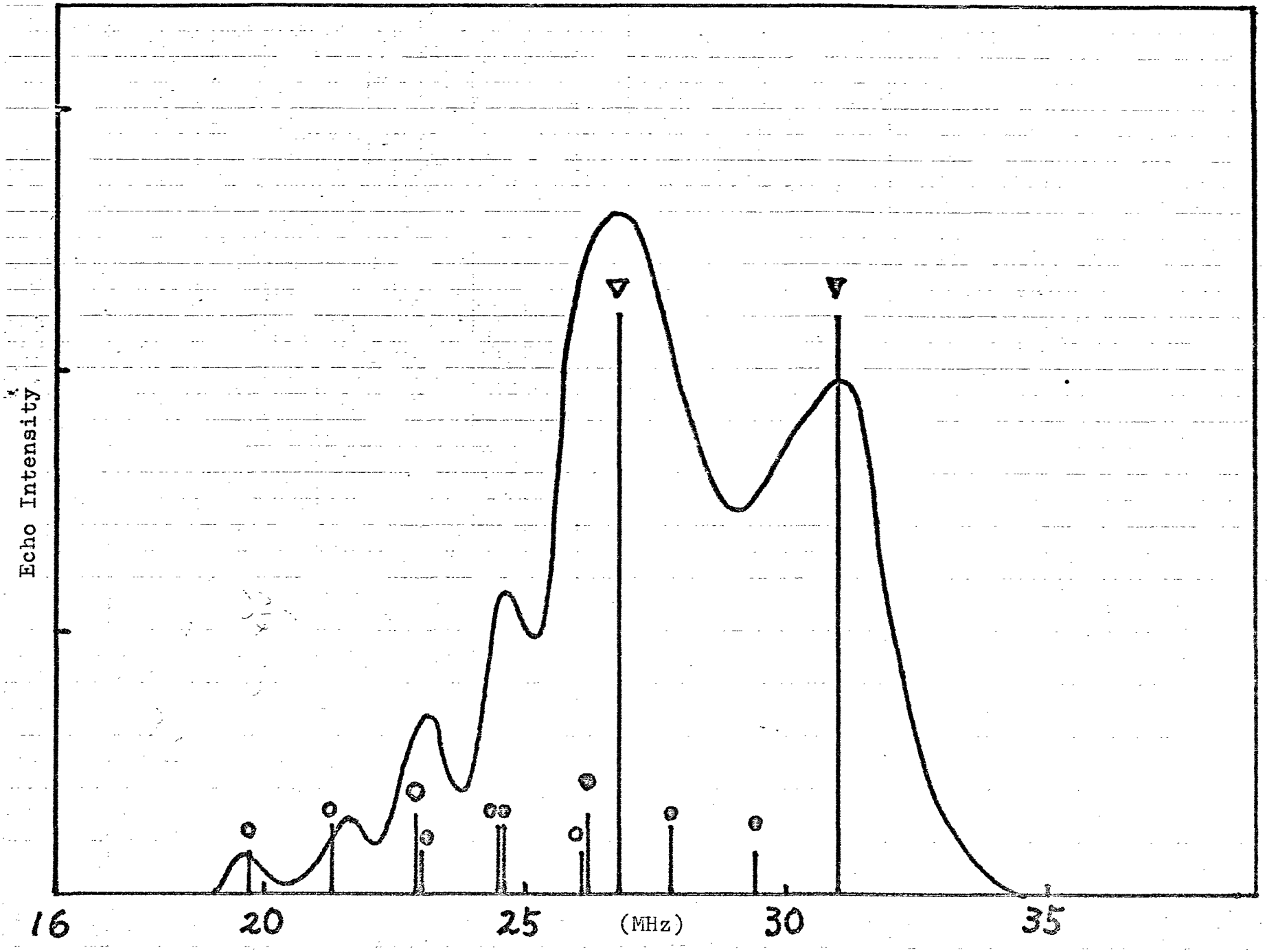
Echo Intensity
16
20
25
(MHz)
30
35